3D UAV Trajectory and Communication Design for Simultaneous Uplink and Downlink Transmission

Meng Hua, *Student Member, IEEE,* Luxi Yang, *Senior Member, IEEE,* Qingqing Wu, *Member, IEEE,* and A. Lee Swindlehurst, *Fellow, IEEE*

***Abstract*—In this paper, we investigate the unmanned aerial vehicle (UAV)-aided simultaneous uplink and downlink transmission networks, where one UAV acting as a disseminator is connected to multiple access points, and the other UAV acting as a base station (BS) collects data from numerous sensor nodes. The goal of this paper is to maximize the sum of the UAV-BS and UAV-AP system throughput by jointly optimizing the 3D UAV trajectory, communication scheduling, and UAV-AP/SN transmit power. We first consider a special case where the UAV-BS and UAV-AP trajectories are pre-determined. Although the resulting problem is an integer and non-convex optimization problem, a globally optimal solution is obtained by applying the polyblock outer approximation (POA) method based on the problem's hidden monotonic structure. Subsequently, for the general case considering the 3D UAV trajectory optimization, an efficient iterative algorithm is proposed to alternately optimize the divided sub-problem based on the successive convex approximation (SCA) technique. Numerical results demonstrate that the proposed design is able to achieve significant system throughput gain over the benchmarks. In addition, the SCA-based method can achieve nearly the same performance as the POA based method with much lower computational complexity.**

***Index Terms*—UAV, communication design, IoT, 3D trajectory optimization, monotonic optimization.**

I. Introduction

With continuing communication device miniaturization and the increased endurance of unmanned aerial vehicles (UAVs), new civilian-use markets are emerging for UAVs beyond military applications, including examples such as emergency search, forest fire detection, cargo transport, etc. Amazon is launching a prime air program that aims to use UAVs to deliver packages to customers [1]. In addition, UAVs are envisioned as a key component of future wireless network technologies that will expand network coverage and improve system throughput [2]. Compared with terrestrial base stations (BSs) whose the locations are pre-determined and fixed, UAVs can adaptively control its position to react as needed to requests for on-demand services [3]–[9].

In the UAV-aided wireless communication scenario, UAV generally acts as a mobile BS equipped with a communication transceiver to provide seamless wireless services or to collect the data from the ground nodes. UAVs are especially well suited for data collection in sensor networks where the nodes are widely dispersed over a large area [10]–[13]. The sensor nodes (SNs) are typically battery operated, and cannot transmit continuously. Rather than installing dedicated infrastructure, in delay-tolerant applications it is more cost effective to deploy UAVs to visit the SNs and collect the data in a sense-and-carry fashion. In addition, the UAV can extend the coverage range or fill in coverage gaps for a given BS, or provide cellular services to ground-based users in remote areas where no infrastructure exists [14]–[16]. Such UAVs can achieve high data rates with low latency due to the high probability of dominant line-of-sight (loS) propagation paths with its communication targets.

Despite promising opportunities for UAVs like those mentioned above, some key challenges remain to be addressed in order to effectively use them to realize seamless connectivity and ultra reliable communication in the future. Recently, UAV deployment and trajectory designs for sensing and communications have received great attention [17]–[26]. The deployment of a single UAV was investigated in [17] and [18] for either maximizing the number of covered users or increasing radio coverage. The deployment of multiple UAVs for either maximizing the coverage area or system throughput was investigated in [19] and [20], respectively. In addition, the authors in [21] studied the deployment of multiple UAVs for providing communication services to SNs in unknown locations, and proposed a game-theory-based method to solve this problem. 2D UAV trajectory optimization was considered in [22], where the authors divided the continuous trajectory into multiple discrete segments and solved the discrete problem by convex optimization techniques. Then, 3D trajectory design has been studied in [23] and [24]. The goal of [23] was to maximize the minimum average data collection rate from all SNs by optimizing the 3D UAV trajectory under the assumption of Rician fading channels, while the optimal 3D trajectory was obtained by applying monotonic optimization theory in [24]. The problem of multiple UAVs simultaneously serving multiple SNs was first studied in [25] and [26]. In [25], the UAV transmit power and trajectory were optimized to alleviate the interference received by the SNs and maximize the minimum achieved rate from all the SNs. In [26], the authors studied multiple-UAV cooperative secure transmission problem by jointly optimizing the UAV trajectory and transmit power.

While the above work has studied the typical UAV-aided wireless communication network either in the uplink transmission or downlink transmission, question of how to integrate the operation of simultaneous uplink and downlink transmission

M. Hua, and L. Yang are with the School of Information Science and Engineering, Southeast University, Nanjing 210096, China (e-mail: {mhua, lxyang}@seu.edu.cn).

Q. Wu is with the Department of Electrical and Computer Engineering, National University of Singapore, Singapore.(e-mail: elewuqq@nus.edu.sg).

A. L. Swindlehurst is with the Center for Pervasive Communications and Computing, University of California at Irvine, Irvine, CA 92697 USA (e-mail: swindle@uci.edu).

has not been addressed and remains an open problem. To fill this gap, we study a general heterogeneous situation where both of these networks are active simultaneously. For the downlink transmission network, UAV acts as a disseminator, referred to as a UAV-AP, to disseminate data to the ground access point (AP) (Note that the AP is also a type of SNs, we name it as AP to distinguish uplink SNs). For the UAV-BS based network, the UAV acts as a mobile base station (BS), referred to as UAV-BS, to collect data from the uplink SNs. We aim to maximize the sum system throughput, including contributions from both UAV-BS and UAV-AP operations, by jointly optimizing the 3D UAV-BS/UAV-AP trajectory, communication scheduling, and UAV-AP/SN transmit power. We propose an efficient iterative algorithm to address the problem and obtain a locally optimal solution. In addition, for the special case where both UAVs' trajectories are pre-determined, we obtain a globally optimal solution by applying monotonic optimization theory.

As shown in Fig. 1, several challenges must be addressed in order to achieve good performance for the simultaneous uplink and downlink transmission with help of UAVs. First, in the UAV-AP based network, namely downlink transmission, the AP not only receives the desired signal from the UAV-AP but also suffers from interference from the SNs. Second, in the UAV-BS based network, namely uplink transmission, the UAV-BS not only collects desired data from the SNs but also encounters interference from the UAV-AP. To enhance system performance, the UAV-BS/UAV-AP trajectories must be carefully designed since the UAV location determines its ability to mitigate interference and increase throughput. Furthermore, transmission power of UAV-AP and SN should be jointly optimized to alleviate the whole system interference. Note that this work is different from work [27], where a single full-duplex UAV is used to transmit data to the downlink users and receive data from the uplink users simultaneously. In this paper, we consider multiple half-duplex UAVs to simultaneously serve downlink APs and uplink SNs, the optimization of 3D trajectory and UAV transmit power is studied. In addition, we propose a novel method to address the resulting problem, and a globally optimal solution is obtained here. It is also worth pointing out that work [25] only focuses on the case of multiple UAVs serving multiple users in the downlink transmission, whereas the uplink transmission is not considered. To the best of our knowledge, this work is first to study simultaneous uplink and downlink transmission with help of multiple UAVs.

Our main contributions are summarized as follows.

- We investigate the scenario of simultaneous uplink and downlink transmission with help of multiple UAVs. We focus on maximizing the sum of the UAV-BS and UAV-AP based network throughput subject to the constraints of UAV mobility and SN/UAV-AP transmit power.
- We first study the case that the UAV-BS and UAV-AP trajectories are pre-determined. We aim at maximizing the sum system throughput by jointly optimizing the SN/UAV-AP transmit power and communication scheduling. The resulting optimization problem is a non-convex integer optimization problem, whose solution is difficult to obtain. However, by exploiting the hidden monotonic nature of the problem, we find a globally optimal solution using the polyblock outer approximation (POA) method. Note that although [24] obtains a globally optimal solution to solar-Powered UAV systems using POA method, it only focuses on a single UAV in the downlink transmission, we extend it to a more general case with multiple UAVs in the simultaneous uplink and downlink transmission. In addition, we also propose a suboptimal solution based on the successive convex approximation (SCA) technique. Our numerical results show that the SCA-based method can achieve nearly the same system performance as the POA-based method but with much lower computational complexity.
- We then study a more general scenario in which the UAV-BS and UAV-AP trajectories are optimized. Our goal is to maximize the sum system throughput by jointly designing the UAV-BS/UAV-AP trajectories, SN/UAV-AP transmit power, and communication scheduling. The resulting optimization problem is much more challenging to solve. Nevertheless, we decompose the problem into three sub-problems: communication scheduling with fixed transmit power and UAV trajectory sub-problem, UAV trajectory with fixed transmit power and communication scheduling sub-problem, and transmit power with fixed UAV trajectory and communication scheduling sub-problem. A three-layer iterative algorithm is then proposed to alternately optimize the communication scheduling, UAV trajectory, and transmit power based on the SCA method.
- To demonstrate our designs more clearly, we consider two simulation scenarios. In the first scenario, one UAV-BS collects data from one SN and one UAV-AP transmits its own data to one AP. In the second scenario, the UAV-BS and UAV-AP simultaneously serve multiple SNs and APs. The impact of the weighting factors, UAV trajectory, and transmit power on the system performance are also studied to reveal useful insights. Numerical results show that our proposed scheme achieves significantly higher system throughput compared with other benchmarks.

The rest of the paper is organized as follows. In Section II, we introduce our system model and formulate the system throughput maximization problem. Section III studies the optimal communication design problem. Section IV investigates the joint 3D UAV trajectory and communication design problem. In Section V, numerical results are presented to illustrate the superiority of our scheme. Finally, Section VI concludes the paper.

II. System Model

We consider an integrated network which consists of a UAV-AP and a UAV-BS based network as shown in Fig. 1. Without loss of generality, we assume that there are K SNs and L APs, which are in fixed locations. The SN and AP sets are respectively denoted as $\mathcal{K}$ and $\mathcal{L}$. The horizontal coordinates of the k-th SN and l-th AP are respectively denoted as $\mathbf{w}_{bk}, k \in \mathcal{K}$ and $\mathbf{w}_{ul}, l \in \mathcal{L}$. We assume that the UAVs can adjust their heading as needed. The period T is equally divided into N

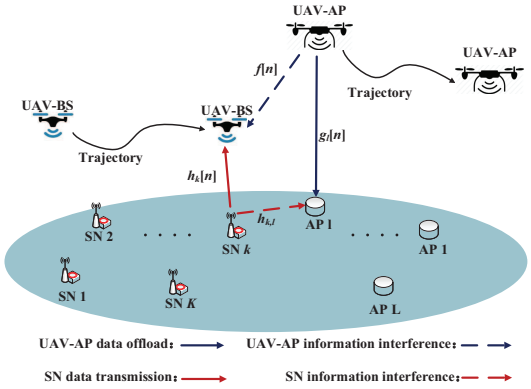

Fig. 1. UAV-aided simultaneous uplink and downlink transmission.

time slots indexed by $n = 1, ..., N$, with duration δ, so that $\delta = \frac{T}{N}$. As a result, the 3D UAV-AP location at any time slot n is denoted by $\mathbf{w}_u[n] = [\mathbf{q}_u[n] \;\; H_u[n]]$, where $\mathbf{q}_u[n]$ and $H_u[n]$ denote the horizontal UAV-AP location and altitude, respectively. Similarly, the 3D UAV-BS location at any time slot n is denoted by $\mathbf{w}_b[n] = [\mathbf{q}_b[n] \;\; H_b[n]]$, where $\mathbf{q}_b[n]$ and $H_u[n]$ denote the horizontal UAV-BS location and altitude, respectively.

Field measurements from Qualcomm have shown that the free space path loss model is appropriate for the UAV when its altitude is beyond a threshold such as 90 meters [28]. In addition, the LoS aerial channel model is also one of the models in the recent 3GPP specification [29]. Following [30]–[34], the channel gain from UAV-AP to UAV-BS is expressed as

$$f[n] = \frac{\beta_0}{\|\mathbf{w}_u[n] - \mathbf{w}_b[n]\|^2}, \tag{1}$$

where β_0 denotes the channel power at the reference distance of 1 meter. Similarly, the channel gain from UAV-AP to l-th AP at time slot n is $g_l[n] = \frac{\beta_0}{\|\mathbf{q}_u[n] - \mathbf{w}_{ul}\|^2 + H_u^2[n]}$, and from the k-th SN to UAV-BS at time slot n is $h_k[n] = \frac{\beta_0}{\|\mathbf{q}_b[n] - \mathbf{w}_{bk}\|^2 + H_b^2[n]}$. In addition, the channel gain from k-th SN to l-th AP follows Rayleigh fading, which is given by

$$h_{k,l} = \tilde{h}_{k,l}\xi = \frac{\beta_0}{\|\mathbf{w}_{bk} - \mathbf{w}_{ul}\|^{\alpha}}\xi, \tag{2}$$

where $\tilde{h}_{k,l} = \frac{\beta_0}{\|\mathbf{w}_{bk} - \mathbf{w}_{ul}\|^{\alpha}}$ stands for the large-scale path loss, α represents the path loss exponent, and ξ is an exponential random variable with mean 1.

To facilitate the system design, we assume the widely used wake-up communication scheduling approach [25], [26], and [33], where the UAV-BS (UAV-AP) can only communicate with at most one SN (AP) in any time slot n. Define the indicator variable $y_k[n], \forall k, n$ and $x_l[n], \forall l, n$ for the UAV-BS and UAV-AP based network, respectively. The UAV-BS serves the k-th SN if $y_k[n] = 1$, otherwise, $y_k[n] = 0$. Similarly, if $x_l[n] = 1$, the UAV-AP migrates the data to the l-th AP, and no data is transmitted if $x_l[n] = 0$. Thus, we have the following communication scheduling constraints

$$\sum\nolimits_{l=1}^{L} x_l[n] \le 1, \;\; x_l[n] \in \{0,1\}, \forall l, n, \tag{3}$$

$$\sum\nolimits_{k=1}^{K} y_k[n] \le 1, \;\; y_k[n] \in \{0,1\}, \forall k, n. \tag{4}$$

If the l-th AP is awakened to communicate with the UAV-AP at time slot n, the achievable downlink ergodic rate of the l-th AP is given by

$$R_l^u[n] = \mathbb{E}\left\{\log_2\left(1 + \frac{g_l[n]p^u[n]}{\sum_{k=1}^{K} h_{k,l}y_k[n]\,p_k^s[n] + \sigma^2}\right)\right\}, \tag{5}$$

where $p^u[n]$ and $p_k^s[n]$ respectively denote the UAV-AP and k-th SN transmit power at time slot n, and σ^2 represents the received noise power.

An exact derivation of (5) is hard to achieve, so instead we formulate a closed-form expression for a lower bound on (5):

$$R_l^{u,lb}[n] = \log_2\left(1 + \frac{g_l[n]p^u[n]}{\sum_{k=1}^{K} \tilde{h}_{k,l}y_k[n]\,p_k^s[n] + \sigma^2}\right), \tag{6}$$

where it follows from the convexity of the function and Jensen's inequality.

When $y_k[n] = 1$, the transmission rate of SN k is given by

$$R_k^s[n] = \log_2\left(1 + \frac{h_k[n]\,p_k^s[n]}{\sum_{l=1}^{L} f[n]\,x_l[n]\,p^u[n] + \sigma^2}\right). \tag{7}$$

Obviously, (7) can be simplified as

$$R_k^s[n] = \log_2\left(1 + \frac{h_k[n]\,p_k^s[n]}{f[n]\,p^u[n] + \sigma^2}\right). \tag{8}$$

This is because with (3), if the AP l is communicated with UAV-AP in time slot n, namely $x_l[n] = 1$, we have $\sum_{l=1}^{L} f[n]\,x_l[n]\,p^u[n] = f[n]\,p^u[n]$; if no AP is activated, the transmission power of UAV-AP $p_u[n]$ must be zero.

In this paper, we focus on the joint design of the UAV trajectory, communication scheduling, and transmit power to maximize the integrated network throughput, i.e., the sum throughput of the UAV-BS and UAV-AP based networks. Define sets $A = \{x_l[n], y_k[n], \forall l, k, n\}$, $P = \{p^u[n], p_k^s[n], \forall k, n\}$, and $Q = \{\mathbf{w}_u[n], \mathbf{w}_b[n], \forall n\}$. Then, the problem can be formulated as

$$\max_{A,P,Q} \beta_1 \sum_{n=1}^{N}\sum_{k=1}^{K} y_k[n]\log_2\left(1 + \frac{h_k[n]\,p_k^s[n]}{f[n]\,p^u[n] + \sigma^2}\right) + \beta_2 \sum_{n=1}^{N}\sum_{l=1}^{L} x_l[n]\log_2\left(1 + \frac{g_l[n]p^u[n]}{\sum_{k=1}^{K} \tilde{h}_{k,l}y_k[n]\,p_k^s[n] + \sigma^2}\right) \tag{9a}$$

$$\text{s.t.} \;\; \sum\nolimits_{l=1}^{L} x_l[n] \le 1, \;\; x_l[n] \in \{0,1\}, \forall l, n, \tag{9b}$$

$$\sum\nolimits_{k=1}^{K} y_k[n] \le 1, \;\; y_k[n] \in \{0,1\}, \forall k, n, \tag{9c}$$

$$0 \le p^u[n] \le p_{\max}^u, \forall n, \tag{9d}$$

$$0 \le p_k^s[n] \le p_{\max}^s, \forall k, n, \tag{9e}$$

$$\|H_i[n] - H_i[n-1]\| \le V_z\delta, \forall n, i \in \{b, u\}, \tag{9f}$$

$$H_{\min} \le H_i[n] \le H_{\max}, \forall n, i \in \{b, u\}, \tag{9g}$$

$$H_i[0] = H_{I_i}, H_i[N] = H_{F_i}, i \in \{b, u\}, \tag{9h}$$

$$\|\mathbf{q}_i[n] - \mathbf{q}_i[n-1]\| \le V_{xy}\delta, \forall n, i \in \{b, u\}, \tag{9i}$$

$$\mathbf{q}_i[0] = \mathbf{q}_{I_i}, \mathbf{q}_i[N] = \mathbf{q}_{F_i}, i \in \{b, u\}, \tag{9j}$$

$$\|\mathbf{q}_b[n] - \mathbf{q}_u[n-1]\|^2 + \|H_b[n] - H_u[n]\|^2 \ge d_{\min}^2, \forall n, \tag{9k}$$

where β_1 and β_2 are the weighting factors. Equations (9d) and (9e) represent the transmit power constraints, with $p^u_{\max}$ and $p^s_{\max}$ denoting the maximum power limits at the UAV-AP and SNs, respectively. Equations (9f)-(9j) denotes the UAV trajectory constraints, where V_z and V_{xy} respectively denote the maximum UAV vertical and horizontal speed, H_{I_i} and $\mathbf{q}_{I_i}$ represent the initial location for UAV i, H_{F_i} and $\mathbf{q}_{F_i}$ represents the final location for UAV i. Finally, (9k) denotes the collision avoidance constraint between the two UAVs with a minimum safety distance $d_{\min}$.

III. Globally optimal communication design

In this section, we obtain a globally optimal solution to (9) for the particular case when the two UAV trajectories are pre-determined. In practice, for a large number of UAV applications, the flight paths are fixed, e.g., the UAV flies in a circular path along the cell edge to serve the cell-edge users, or the UAV flies in a straight line to communicate with the ground users [31], [35]. As a result, (9) is simplified as

$$\max_{A,P} \beta_1 \sum_{n=1}^{N}\sum_{k=1}^{K} y_k[n]\log_2\left(1+\frac{h_k[n]\,p^s_k[n]}{f[n]\,p^u[n]+\sigma^2}\right)+ \beta_2 \sum_{n=1}^{N}\sum_{l=1}^{L} x_l[n]\log_2\left(1+\frac{g_l[n]p^u[n]}{\sum_{k=1}^{K}\tilde{h}_{k,l}y_k[n]\,p^s_k[n]+\sigma^2}\right) \tag{10a}$$

s.t. (9b)-(9e).

Problem (10) is difficult to solve due to the coupled power and communication scheduling in (10a) and the binary variables in (9b) and (9c). However, we show how to optimally solve (10) by using monotonic optimization theory [36], [37]. First, it is observed that $y_k[n]$ and $x_l[n]$ in (10) can be moved into the numerator of the logarithm terms since $y_k[n] = 1$ for at most one SN k ($x_l[n] = 1$ for at most one AP l). Either way, the terms where $y_k[n] = 0$ and $x_l[n] = 0$ do not contribute to the objective value. Defining $\tilde{p}^u_l[n] = p^u[n]\,x_l[n]$ for all l, $\tilde{p}^s_k[n] = p^s_k[n]\,y_k[n]$ for all k, and $\tilde{P} = \{\tilde{p}^u[n], \tilde{p}^s_k[n], \forall k, n\}$, we formulate the following problem:

$$\max_{\tilde{P}} \beta_1 \sum_{n=1}^{N}\sum_{k=1}^{K} \log_2\left(1+\frac{h_k[n]\,\tilde{p}^s_k[n]}{M\sum_{i\neq k}^{K}\tilde{p}^s_i[n]+\sum_{l=1}^{L} f[n]\,\tilde{p}^u_l[n]+\sigma^2}\right) + \beta_2 \sum_{n=1}^{N}\sum_{l=1}^{L} \log_2\left(1+\frac{g_l[n]\tilde{p}^u_l[n]}{M\sum_{i\neq l}^{L}\tilde{p}^u_i[n]+\sum_{k=1}^{K}\tilde{h}_{k,l}\tilde{p}^s_k[n]+\sigma^2}\right) \tag{11a}$$

$$\text{s.t. } \tilde{P}\in\mathcal{P}, \tag{11b}$$

where $\mathcal{P} = \left\{\tilde{P} | 0\le \tilde{p}^u_l[n]\le p^u_{\max}, 0\le \tilde{p}^s_k[n]\le p^s_{\max}, \forall k,l,n\right\}$ and M is a sufficiently large penalty factor.

Theorem 1: Problem (11) is equivalent to (10).

Proof: Please refer to Appendix A. ∎

There is no standard method to obtain the optimal solution to (11) due to the coupled transmit power in the objective function. However, by exploiting the hidden monotonicity in the problem, we obtain the optimal solution to problem (11) by following two steps. We first transform the problem (11) into an equivalent canonical monotonic optimization formulation. Then, we apply a sequence of ploybloks to approach the optimal vertex using the polyblock outer approximation method. Specifically, by introducing the auxiliary variables $\chi_k[n]$ and $\bar{\chi}_l[n]$, problem (11) can be equivalently written as

$$\max_{\chi_k[n],\bar{\chi}_l[n]} \beta_1 \sum_{n=1}^{N}\sum_{k=1}^{K}\log_2\left(1+\chi_k[n]\right) + \beta_2 \sum_{n=1}^{N}\sum_{l=1}^{L}\log_2\left(1+\bar{\chi}_l[n]\right) \tag{12a}$$

$$\text{s.t. } \left(\boldsymbol{\chi}_k[n], \bar{\boldsymbol{\chi}}_l[n]\right)\in\mathcal{G}, \tag{12b}$$

where $\boldsymbol{\chi}_k[n]$ and $\bar{\boldsymbol{\chi}}_l[n]$ are the collections of the $\chi_k[n]$ and $\bar{\chi}_l[n]$, respectively, and the normal set $\mathcal{G}$ is defined in (13). Note that the signal-to-interference-plus-noise-ratio (SINR) for the UAV-BS and UAV-AP based networks must be non-negative. Therefore, both $\chi_k[n]$ and $\bar{\chi}_l[n]$ must be no smaller than than zero, i.e., $\mathcal{H}=\{(\chi_k[n],\bar{\chi}_l[n])\,|\chi_k[n]\ge 0,\bar{\chi}_l[n]\ge 0,\forall k,l,n\}$.

Since the objective function in (12) is an increasing function with $\chi_k[n]$ and $\bar{\chi}_l[n]$, (12) can be globally solved by finding the upper boundary of the feasible set using the POA method, which is summarized in Algorithm 1. In the initial stage, we set $\chi^1_k[n] = \frac{h_k[n]p^s_{\max}}{\sigma^2}$ and $\bar{\chi}^1_l[n] = \frac{g_l[n]p^u_{\max}}{\sigma^2}$ for $\forall k,l,n$; $\mathcal{T}^1=\{\boldsymbol{v}^1\}$, maximum tolerance $\epsilon = 10^{-2}$, and iterative index $t=1$.

Algorithm 1 Polyblock Outer Approximation (POA) based method

1: **Initialize** polyblock $\mathcal{S}^1$ with vertex $\boldsymbol{v}^1 = (\boldsymbol{\chi}^1_k[n], \bar{\boldsymbol{\chi}}^1_l[n])$, where $\chi^1_k[n] = \frac{h_k[n]p^s_{\max}}{\sigma^2}$ and $\bar{\chi}^1_l[n] = \frac{g_l[n]p^u_{\max}}{\sigma^2}$ for $\forall k,l,n$; $\mathcal{T}^1=\{\boldsymbol{v}^1\}$, maximum tolerance $\epsilon = 10^{-2}$, and iterative index $t=1$.
2: **Repeat**
3: Compute the projection of $\mathbf{v}^t$ on the upper boundary of $\mathcal{G}$, denoted as $\boldsymbol{\pi}^{\mathcal{G}}(\mathbf{v}^t)$, via Algorithm 2.
4: With $\boldsymbol{\pi}^{\mathcal{G}}(\mathbf{v}^t)$, generate M new vertices $\{\tilde{\mathbf{v}}^t_1,...,\tilde{\mathbf{v}}^t_M\}$, where $\tilde{\mathbf{v}}^t_i = \mathbf{v}^t - \left(v^t_i - \boldsymbol{\pi}^{\mathcal{G}}_i(\mathbf{v}^t)\right)\mathbf{e}_i$ for $i=1,...,M$.
5: Construct a smaller polyblock $\mathcal{S}^{t+1}$ with vertex set $\mathcal{T}^{t+1}$ by replacing $\mathbf{v}^t$ in $\mathcal{T}^t$ with M new vertices $\{\tilde{\mathbf{v}}^t_1,...,\tilde{\mathbf{v}}^t_M\}$.
6: Find $\mathbf{v}^{t+1}$ as the candidate vertex that maximizes the objective function of problem (12) over set $\mathcal{T}^{t+1}\cap\mathcal{H}$.
7: $t = t+1$.
8: **Until** $\max_i\left\{\frac{\|\mathbf{v}^t_i-\boldsymbol{\pi}^{\mathcal{G}}_i(\mathbf{v}^t)\|}{\|\mathbf{v}^t_i\|}\right\}\le\epsilon$.
9: Output optimal transmit power $\{\tilde{p}^{s,*}_k[n]\}$ and $\{\tilde{p}^{u,*}_l[n]\}$ by computing $\boldsymbol{\pi}^{\mathcal{G}}(\mathbf{v}^t)$ in Algorithm 2.

$\chi^1_k[n] = \frac{h_k[n]p^s_{\max}}{\sigma^2}$ and $\bar{\chi}^1_l[n] = \frac{g_l[n]p^u_{\max}}{\sigma^2}$ for $\forall k,l,n$, it is clear that polyblock $\mathcal{S}^1$ is a box $\left[\mathbf{0}\ \mathbf{v}^1\right]$ comprising the normal set $\mathcal{G}$. In step 4, $M=(K+L)N$ stands for the number of variables, v^t_i is the ith element of $\boldsymbol{v}^t$, $\boldsymbol{\pi}^{\mathcal{G}}_i(\mathbf{v}^t)$ is the ith element of $\boldsymbol{\pi}^{\mathcal{G}}(\mathbf{v}^t)$, and $\boldsymbol{e}_i$ denotes the ith column of the identity matrix. In steps 3-6, we shrink the polyblocks $\mathcal{S}^1\supset\mathcal{S}^2\supset\cdots\supset\mathcal{G}$ to approximate the feasible set to find the optimal upper boundary point of the bounded normal set. Note that the complexity of Algorithm 1 is difficult to evaluate in general since it mainly depends on the number of iterations required to search the boundary of the feasible set (i.e., step 3) and on computation of the objective value for all vertices (i.e., step 6). However, in the worst case, the computational complexity of Algorithm 1 grows exponentially with M [38].

$$\mathcal{G}=\left\{\left(\chi_k\left[n\right],\bar{\chi}_l\left[n\right]\right)|\chi_k\left[n\right]\leq\frac{h_k\left[n\right]\tilde{p}_k^s\left[n\right]}{M\sum_{i\neq k}^{K}\tilde{p}_i^s\left[n\right]+\sum_{l=1}^{L}f\left[n\right]\tilde{p}_l^u\left[n\right]+\sigma^2},\bar{\chi}_l\left[n\right]\leq\frac{g_l[n]\tilde{p}_l^u\left[n\right]}{M\sum_{i\neq l}^{L}\tilde{p}_i^u\left[n\right]+\sum_{k=1}^{K}\tilde{h}_{k,l}\tilde{p}_k^s\left[n\right]+\sigma^2},\forall l,k,n,\tilde{P}\in\mathcal{P}\right\}. \tag{13}$$

Following [37], the value $\boldsymbol{\pi}^{\mathcal{G}}\left(\mathbf{v}^t\right)$ in step 3 of Algorithm 1 can be calculated as follows: $\pi^{\mathcal{G}}\left(\mathbf{v}^t\right)=\lambda\mathbf{v}^t$, where $\lambda=\max\left\{a|a\mathbf{v}^t\in\mathcal{G}\right\}$, and the details are summarized in Algorithm 2.

Algorithm 2 Bisection Search to Compute $\boldsymbol{\pi}^{\mathcal{G}}\left(\mathbf{v}^t\right)$

1: **Initialize:** $\lambda_{\min}=0$, $\lambda_{\max}=1$, $\epsilon=10^{-2}$.
2: **Repeat**
3: Compute $\lambda=\frac{\lambda_{\min}+\lambda_{\max}}{2}$
4: Check the feasibility of problem (14), i.e., $\lambda\mathbf{v}^t\in\mathcal{G}$. If yes, let $\lambda_{\min}=\lambda$, otherwise, let $\lambda_{\max}=\lambda$.
5: **Until** $\lambda_{\max}-\lambda_{\min}\leq\epsilon$
6: Output $\lambda=\lambda_{\min}$ and $\pi^{G}\left(\mathbf{v}^t\right)=\lambda\mathbf{v}^t$. The optimal power allocation $\{\tilde{p}_k^{s,*}\left[n\right]\}$ and $\{\tilde{p}_l^{u,*}\left[n\right]\}$ are obtained by solving problem (14) for $\lambda=\lambda_{\min}$.

$$\text{Find solutions}:\{\tilde{p}_k^s\left[n\right],\tilde{p}_l^u\left[n\right]\}$$

$$\text{s.t. }\lambda\chi_k\left[n\right]\leq\frac{h_k\left[n\right]\tilde{p}_k^s\left[n\right]}{M\sum_{i\neq k}^{K}\tilde{p}_i^s\left[n\right]+\sum_{l=1}^{L}f\left[n\right]\tilde{p}_l^u\left[n\right]+\sigma^2}, \tag{14a}$$

$$\lambda\bar{\chi}_l\left[n\right]\leq\frac{g_l[n]\tilde{p}_l^u\left[n\right]}{M\sum_{i\neq l}^{L}\tilde{p}_i^u\left[n\right]+\sum_{k=1}^{K}\tilde{h}_{k,l}\tilde{p}_k^s\left[n\right]+\sigma^2}. \tag{14b}$$

$$0\leq\tilde{p}_l^u\left[n\right]\leq p_{\max}^u,\forall n, \tag{14c}$$

$$0\leq\tilde{p}_k^s\left[n\right]\leq p_{\max}^s,\forall k,n. \tag{14d}$$

Note that (14) can become a linear optimization problem by transforming the fractional constraints (14a) and (14b) into linear forms, and thus can be optimally solved. Then, we can recover the optimal transmit power for (10) using the following steps: if $\tilde{p}_k^s\left[n\right]>0$, $y_k[n]=1$ and $p_k^s\left[n\right]=\tilde{p}_k^s\left[n\right]$; and if $\tilde{p}_k^s\left[n\right]=0$, $y_k[n]=0$ and $p_k^s\left[n\right]=0$. Similar to $p_l^u\left[n\right]$, if $\tilde{p}_l^u\left[n\right]>0$, $x_l[n]=1$ and $p_l^u\left[n\right]=\tilde{p}_l^u\left[n\right]$; and if $\tilde{p}_l^u\left[n\right]=0$, $x_l[n]=0$ and $p_l^u\left[n\right]=0$.

Although we obtain a globally optimal solution for (10) using the POA method, the computational complexity is very high. To address this issue, a lower-complexity SCA-method can be used as discussed in the next section.

IV. Joint 3D trajectory and communication design optimization

In this section, we investigate the joint 3D trajectory and communication design optimization for maximizing the system throughput using the low-complexity SCA method. Problem (9) is a mixed integer and non-convex optimization problem due to the objective function (9a) and constraints (9b), (9c), and (9k). We decompose problem (9) into three sub-problems, and then optimize each sub-problem in an iterative way. Specifically, the three sub-problems are the communication scheduling optimization with fixed transmit power and 3D UAV trajectory; the 3D UAV trajectory optimization with fixed transmit power and communication scheduling; the transmit power optimization with fixed communication scheduling and 3D UAV trajectory. First, we relax the integer communication scheduling constraints (9b) and (9c) into continuous constraints as

$$\sum\nolimits_{l=1}^{L}x_l\left[n\right]\leq1,\ 0\leq x_l\left[n\right]\leq1,\forall l,n, \tag{15}$$

$$\sum\nolimits_{k=1}^{K}y_k\left[n\right]\leq1,\ 0\leq y_k\left[n\right]\leq1,\forall k,n, \tag{16}$$

A. Communication scheduling optimization with fixed transmit power and trajectory

For any given Q and P, the communication scheduling subproblem is given by

$$\max_{y_k[n],x_l[n]}\beta_1\sum_{n=1}^{N}\sum_{k=1}^{K}y_k\left[n\right]\log_2\left(1+\frac{h_k\left[n\right]p_k^s\left[n\right]}{f\left[n\right]p^u\left[n\right]+\sigma^2}\right)+\beta_2\sum_{n=1}^{N}\sum_{l=1}^{L}x_l[n]\log_2\left(1+\frac{g_l[n]p^u\left[n\right]}{\sum_{k=1}^{K}\tilde{h}_{k,l}y_k\left[n\right]p_k^s\left[n\right]+\sigma^2}\right) \tag{17a}$$

$$\text{s.t. (15), (16).}$$

As can be seen, the second term of (17a) is convex but not concave w.r.t to $y_k[n]$, which makes problem (17) non-convex. To tackle it, we apply the SCA method [39]. Specifically, for any feasible point $y_k^r[n]$ in the r-th iteration, we have

$$R_l^{u,lb}\left[n\right]\geq\log_2\left(1+\frac{g_l[n]p^u\left[n\right]}{\sum_{k=1}^{K}\tilde{h}_{k,l}y_k^r\left[n\right]p_k^s\left[n\right]+\sigma^2}\right)-\sum\nolimits_{k=1}^{K}A_k^l\left(y_k\left[n\right]-y_k^r\left[n\right]\right)\triangleq\varphi^{lb}\left(R_l^{u,lb}\left[n\right]\right), \tag{18}$$

where $A_k^l=\frac{g_l[n]p^u[n]\tilde{h}_{k,l}p_k^s[n]\log_2e}{\left(\sum_{k=1}^{K}\tilde{h}_{k,l}y_k^r[n]p_k^s[n]+\sigma^2\right)\left(\sum_{k=1}^{K}\tilde{h}_{k,l}y_k^r[n]p_k^s[n]+\sigma^2+g_l[n]p^u[n]\right)}$.
Obviously, $\varphi^{lb}\left(R_l^{u,lb}\left[n\right]\right)$ is linear with $y_k[n]$, which is convex. Therefore, the value $y_k^{r+1}[n]$ in the $r+1$-th iteration can be achieved by solving the following convex problem:

$$\max_{y_k[n]}\beta_1\sum_{n=1}^{N}\sum_{k=1}^{K}y_k\left[n\right]\log_2\left(1+\frac{h_k\left[n\right]p_k^s\left[n\right]}{f\left[n\right]p^u\left[n\right]+\sigma^2}\right)+\beta_2\sum_{n=1}^{N}\sum_{l=1}^{L}\varphi^{lb}\left(R_l^{u,lb}\left[n\right]\right) \tag{19a}$$

$$\text{s.t. (15), (16).}$$

By successively updating the $y_k^r[n]$, a locally optimal solution can be found.

$$\psi\left(R_l^{u,lb}[n]\right)=\log_2\left(1+\frac{S_{1,l}[n]}{\left\|\mathbf{q}_u^r[n]-\mathbf{w}_{ul}\right\|^2+H_u^r[n]^2}\right)-S_{2,l}[n]\left(\left\|\mathbf{q}_u[n]-\mathbf{w}_{ul}\right\|^2+H_u[n]^2-\left\|\mathbf{q}_u^r[n]-\mathbf{w}_{ul}\right\|^2-H_u^r[n]^2\right), \tag{23}$$

B. 3D UAV trajectory optimization with fixed transmit power and communication scheduling

For any given A and P, the 3D trajectory problem is given by

$$\max_{Q}\beta_1\sum_{n=1}^{N}\sum_{k=1}^{K}y_k[n]\log_2\left(1+\frac{h_k[n]p_k^s[n]}{f[n]p^u[n]+\sigma^2}\right)+\beta_2\sum_{n=1}^{N}\sum_{l=1}^{L}x_l[n]\log_2\left(1+\frac{g_l[n]p^u[n]}{\sum_{k=1}^{K}\tilde{h}_{k,l}y_k[n]p_k^s[n]+\sigma^2}\right) \tag{20a}$$

s.t.(9f)-(9k).

Problem (20) is non-convex due to the non-convex objective function (20a) and non-convex constraint (9k). Let $\psi\left(R_l^{u,lb}[n]\right)$ be the first order Taylor expansion of $R_l^{u,lb}[n]$ at the feasible point $Z_l^{u,r}[n]\triangleq\left\|\mathbf{q}_u^r[n]-\mathbf{w}_{ul}\right\|^2+H_u^r[n]^2$ in the r-th iteration, given by (23) at the top on the next page, where

$$S_{1,l}[n]=\frac{p^u[n]\beta_0}{\sum_{k=1}^{K}\tilde{h}_{k,l}y_k[n]p_k^s[n]+\sigma^2}, \tag{21}$$

and

$$S_{2,l}[n]=\frac{S_{1,l}[n]}{Z_l^{u,r}[n]\left(Z_l^{u,r}[n]+S_{1,l}[n]\right)}. \tag{22}$$

Equation (23) is concave w.r.t the UAV trajectory variable Q. In addition, $R_k^s[n]$ in (20a) can be rewritten as

$$R_k^s[n]=\hat{R}_k^s[n]-\log\left(\frac{\beta_0p^u[n]}{\left\|\mathbf{w}_u[n]-\mathbf{w}_b[n]\right\|^2}+\sigma^2\right), \tag{24}$$

where

$$\hat{R}_k^s[n]=\log\left(\frac{\beta_0p^u[n]}{\left\|\mathbf{w}_u[n]-\mathbf{w}_b[n]\right\|^2}+\frac{\beta_0p_k^s[n]}{\left\|\mathbf{q}_b[n]-\mathbf{w}_{bk}\right\|^2+H_b[n]^2}+\sigma^2\right). \tag{25}$$

By introducing the slack variables $\Upsilon[n]$, (24) can be recast as

$$R_k^s[n]=\hat{R}_k^s[n]-\log\left(\frac{\beta_0p^u[n]}{\Upsilon[n]}+\sigma^2\right), \tag{26}$$

with the additional constraints

$$0<\Upsilon[n]\le\left\|\mathbf{w}_u[n]-\mathbf{w}_b[n]\right\|^2,\forall n. \tag{27}$$

We can see that the second term $\log\left(\frac{\beta_0p^u[n]}{\Upsilon[n]}+\sigma^2\right)$ in (26) is convex w.r.t. $\Upsilon[n]$. However, the new constraint (27) is non-convex. Let $\psi(\Upsilon[n])$ be the first order Taylor expansion of $\left\|\mathbf{w}_u[n]-\mathbf{w}_b[n]\right\|^2$ at the feasible point $\mathbf{w}_u^r[n]=[\mathbf{q}_u^r[n]\ \ H_u^r[n]]$, $\mathbf{w}_b^r[n]=[\mathbf{q}_b^r[n]\ \ H_b^r[n]]$ in the r-th iteration. Then

$$\psi(\Upsilon[n])=\left\|\mathbf{w}_u^r[n]-\mathbf{w}_b^r[n]\right\|^2+2\left(\mathbf{w}_u^r[n]-\mathbf{w}_b^r[n]\right)\times\left(\mathbf{w}_u[n]-\mathbf{w}_u^r[n]\right)^T-2\left(\mathbf{w}_u^r[n]-\mathbf{w}_b^r[n]\right)\left(\mathbf{w}_b[n]-\mathbf{w}_b^r[n]\right)^T. \tag{28}$$

The constraint (27) can be reformulated as

$$0<\Upsilon[n]\le\psi(\Upsilon[n]),\forall n. \tag{29}$$

Note that the first term $\hat{R}_k^s[n]$ in (26) is also non-convex. To this end, let $\psi\left(\hat{R}_k^s[n]\right)$ be the first order Taylor expansion of $\hat{R}_k^s[n]$ at any feasible points $\left\|\mathbf{w}_u^r[n]-\mathbf{w}_b^r[n]\right\|^2$ and $\left\|\mathbf{q}_b^r[n]-\mathbf{w}_{bk}\right\|^2+H_b^r[n]^2$ in the r-th iteration, given by (30) on the next page, where

$$\Omega_{k,1}[n]=\frac{\frac{\beta_0p^u[n]}{\left\|\mathbf{w}_u^r[n]-\mathbf{w}_b^r[n]\right\|^4}\log_2e}{\frac{\beta_0p^u[n]}{\left\|\mathbf{w}_u^r[n]-\mathbf{w}_b^r[n]\right\|^2}+\frac{\beta_0p_k^s[n]}{\left\|\mathbf{q}_b^r[n]-\mathbf{w}_{bk}\right\|^2+H_b^r[n]^2}+\sigma^2}, \tag{31}$$

and

$$\Omega_{k,2}[n]=\frac{\frac{\beta_0p_k^s[n]}{\left(\left\|\mathbf{q}_b^r[n]-\mathbf{w}_{bk}\right\|^2+H_b^r[n]^2\right)^2}\log_2e}{\frac{\beta_0p^u[n]}{\left\|\mathbf{w}_u^r[n]-\mathbf{w}_b^r[n]\right\|^2}+\frac{\beta_0p_k^s[n]}{\left\|\mathbf{q}_b^r[n]-\mathbf{w}_{bk}\right\|^2+H_b^r[n]^2}+\sigma^2}. \tag{32}$$

In addition, the constraint (9k) is non-convex. With (28), constraint (9k) can be replaced by

$$\psi(\Upsilon[n])\ge d_{\min}^2,\forall n. \tag{33}$$

As a result, with (23) and (30), define the following optimization problem

$$\max_{Q,\Upsilon[n]}\beta_1\sum_{n=1}^{N}\sum_{k=1}^{K}y_k[n]\left(\psi\left(\hat{R}_k^s[n]\right)-\log\left(\frac{\beta_0p^u[n]}{\Upsilon[n]}+\sigma^2\right)\right)+\beta_2\sum_{n=1}^{N}\sum_{l=1}^{L}x_l[n]\psi\left(R_l^{u,lb}[n]\right) \tag{34a}$$

s.t.(9f)-(9j), (29), (33)

Problem (34) can be efficiently solved by standard methods due to its convexity. Then, a locally optimal solution to problem (20) can be guaranteed by successively updating the 3D UAV trajectory obtained from problem (34).

$$\psi\left(\hat{R}_k^s[n]\right)=\log\left(\frac{\beta_0 p^u[n]}{\|\mathbf{w}_u^r[n]-\mathbf{w}_b^r[n]\|^2}+\frac{\beta_0 p_k^s[n]}{\|\mathbf{q}_b^r[n]-\mathbf{w}_{bk}\|^2+H_b^r[n]^2}+\sigma^2\right)-$$
$$\Omega_{k,1}[n]\left(\|\mathbf{w}_u[n]-\mathbf{w}_b[n]\|^2-\|\mathbf{w}_u^r[n]-\mathbf{w}_b^r[n]\|^2\right)-\Omega_{k,2}[n]\left(\|\mathbf{q}_b[n]-\mathbf{w}_{bk}\|^2+H_b[n]^2-\|\mathbf{q}_b^r[n]-\mathbf{w}_{bk}\|^2-H_b^r[n]^2\right), \tag{30}$$

C. Transmit power optimization with fixed communication scheduling and 3D UAV trajectory

For any given A and Q, the transmit power optimization problem is simplified as

$$\max_P \beta_1\sum_{n=1}^{N}\sum_{k=1}^{K}y_k[n]\log_2\left(1+\frac{h_k[n]p_k^s[n]}{f[n]p^u[n]+\sigma^2}\right)+ \beta_2\sum_{n=1}^{N}\sum_{l=1}^{L}x_l[n]\log_2\left(1+\frac{g_l[n]p^u[n]}{\sum_{k=1}^{K}\tilde{h}_{k,l}y_k[n]p_k^s[n]+\sigma^2}\right) \tag{35a}$$
s.t.(9d), (9e).

The objective function (35a) is non-convex. To tackle it, we again apply the SCA method. Specifically, we rewrite $R_k^s[n]$ as

$$R_k^s[n]=\log_2\left(h_k[n]p_k^s[n]+f[n]p^u[n]+\sigma^2\right)-\tilde{R}_k^s[n], \tag{36}$$

where

$$\tilde{R}_k^s[n]=\log_2\left(f[n]p^u[n]+\sigma^2\right). \tag{37}$$

Obviously, (36) is a difference of convex (DC) functions. We replace the term $\tilde{R}_k^s[n]$ by its first order Taylor expansion at any given feasible point $p^{u,r}[n]$, denoted as $\psi\left(\tilde{R}_k^s[n]\right)$, and given by

$$\psi\left(\tilde{R}_k^s[n]\right)=\log_2\left(f[n]p^{u,r}[n]+\sigma^2\right)+ \frac{f[n]\log_2 e}{f[n]p^{u,r}[n]+\sigma^2}\left(p^u[n]-p^{u,r}[n]\right). \tag{38}$$

Next, we tackle the non-convexity of $R_l^{u,lb}[n]$ in (35a) by rewriting $R_l^{u,lb}[n]$ as

$$R_l^{u,lb}[n]=\log_2\left(g_l[n]p^u[n]+\sum\nolimits_{k=1}^{K}\tilde{h}_{k,l}y_k[n]p_k^s[n]+\sigma^2\right)-\tilde{R}_l^{u,lb}[n], \tag{39}$$

where

$$\tilde{R}_l^{u,lb}[n]=\log_2\left(\sum\nolimits_{k=1}^{K}\tilde{h}_{k,l}y_k[n]p_k^s[n]+\sigma^2\right). \tag{40}$$

Interestingly, (39) is also a difference of convex (DC) functions. By taking the same steps as in (36), an upper bound for $\tilde{R}_l^{u,lb}[n]$ at any feasible point $p_k^{s,r}[n]$ is given by

$$\psi\left(\tilde{R}_l^{u,lb}[n]\right)=\log_2\left(\sum\nolimits_{k=1}^{K}\tilde{h}_{k,l}y_k[n]p_k^{s,r}[n]+\sigma^2\right)+ \sum\nolimits_{k=1}^{K}\frac{\tilde{h}_{k,l}y_k[n]}{\sum_{k=1}^{K}\tilde{h}_{k,l}y_k[n]p_k^{s,r}[n]+\sigma^2}\left(p_k^s[n]-p_k^{s,r}[n]\right). \tag{41}$$

Consequently, with (38) and (41), we define the following optimization problem

$$\max_P \beta_1\sum_{n=1}^{N}\sum_{k=1}^{K}y_k[n]\left(\log_2\left(h_k[n]p_k^s[n]+f[n]p^u[n]+\sigma^2\right)-\psi\left(\tilde{R}_k^s[n]\right)\right)+\beta_2\sum_{n=1}^{N}\sum_{l=1}^{L}x_l[n]\left(\log_2\left(g_l[n]p^u[n]+\sum_{k=1}^{K}\tilde{h}_{k,l}y_k[n]p_k^s[n]+\sigma^2\right)-\psi\left(\tilde{R}_l^{u,lb}[n]\right)\right) \tag{42a}$$
s.t.(9d), (9e).

It can be verified that problem (42) is a convex optimization problem, which can be readily solved. Then, a locally optimal solution to problem (35) can be guaranteed by successively updating the transmit power obtained from problem (42).

D. Overall algorithm

To find the solution to the original problem, we optimize these three sub-problems in an iterative way using the block descent (BD) method. The BD method guarantees convergence, and the complexity of the overall algorithm is polynomial in the worst case [20], [25], [40]. Finally, we reconstruct the continuous communication scheduling variables into binary variables using a simple *round function* strategy [27].

V. NUMERICAL RESULTS

In this section, numerical examples are provided to validate the effectiveness of the proposed approach. Unless otherwise specified, the simulation parameters are set as follows. We assume that the system bandwidth is B=1MHz with noise power σ^2= -110dBm [22]. The channel gain is β_0= -60dBm with path loss exponent $\alpha=3$ [31]. The UAV altitude constraints are $H_{\min}$=100m and $H_{\max}$=600m. The maximum horizontal and vertical UAV speed are set to V_{xy}=50m/s and V_z=30m/s, respectively. The minimum safety distance between two UAVs is $d_{\min}$=10m. The maximum UAV-AP and SN transmit power is set as $p_{\max}^s$=0.1W and $p_{\max}^u$=0.1W, respectively. In addition, the duration of each time slot is set as δ=0.5s, and the penalty factor is set as $M=1\times10^5$.

A. Optimal communication design

We first investigate the optimal communication design leveraging the POA method. The locations of the SNs and APs, and the predetermined UAV trajectory are set as follows: 4 SN locations are $\mathbf{w}_{b1}$=[-1000m 0], $\mathbf{w}_{b2}$=[-100m 700m], $\mathbf{w}_{b3}$=[0 0], $\mathbf{w}_{b4}$=[-500m -500m], and 4 AP locations are $\mathbf{w}_{u1}$=[1000m

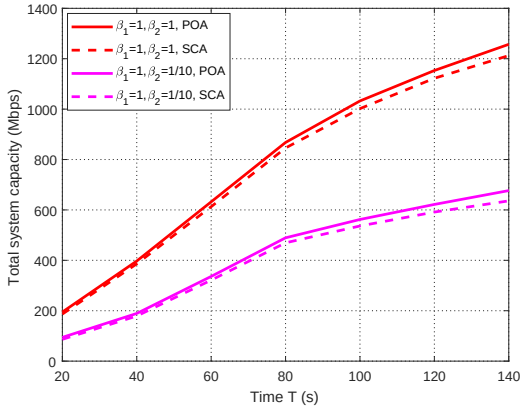

Fig. 2. Total system throughput versus period T for different weighting factors using POA and SCA methods.

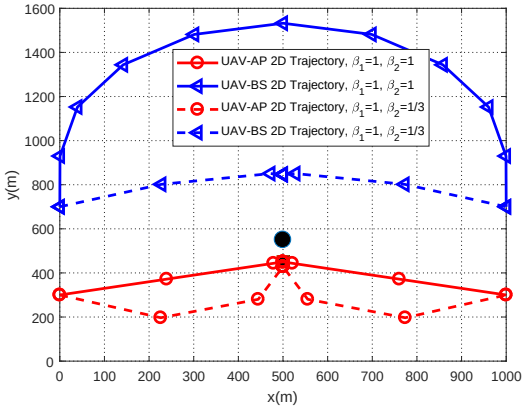

Fig. 3. Optimized UAV trajectories for different weighting factors when $T = 50s$. SN's location is marked by ●. AP's location is marked by ■.

0], $\mathbf{w}_{u2}$=[0 700m], $\mathbf{w}_{u3}$=[100m 0], $\mathbf{w}_{u4}$=[700m -400m]. The initial trajectories for the UAV-BS and UAV-AP are circles with given radii and centers. Specifically, first, for any given period T and maximum UAV horizontal speed V_{xy}, the circle radius is calculated as $r_c = \frac{V_{xy}T}{2\pi}, c \in \{b, u\}$. Second, for any given location of $\mathbf{w}_{ci}, c \in \{b, u\}, i \in \{\mathcal{K}, \mathcal{L}\}$, the geometric center of the SNs and APs are $\mathbf{ge}_b = \frac{\sum_{i=1}^{K} \mathbf{w}_{bi}}{K} = [x_b \ y_b]$ and $\mathbf{ge}_u = \frac{\sum_{i=1}^{L} \mathbf{w}_{ui}}{L} = [x_u \ y_u]$, respectively. The initial trajectories of the UAV-BS and UAV-AP at time slot n are respectively calculated as

$$\mathbf{q}_b[n] = [x_b + r_b \cos(\theta_n + \pi) \ \ y_b + r_b \sin(\theta_n)] \tag{43}$$

and

$$\mathbf{q}_u[n] = [x_u + r_u \cos(\theta_n) \ \ y_u + r_u \sin(\theta_n)], \tag{44}$$

where $\theta_n = \frac{2\pi n}{N}, n = 1, \ldots, N$.

In Fig. 2, we compare the total sum system throughput achieved by the POA and SCA method, versus period T, for different weighting factors. Here, we consider two different weighting factors, for $\beta_1 = 1, \beta_2 = 1$, the priority of the two networks is assumed to be same, and for $\beta_1 = 1, \beta_2 = 1/10$, the priority of UAV-BS-based network is higher than that of UAV-AP-based network. Note that the case for $\beta_1 < \beta_2$ is not considered here since the result insights are similar to the case of $\beta_1 = 1, \beta_2 = 1/10$. As can be seen, when period T is small, namely $T \leq 80s$, the system throughput obtained by the POA and SCA-based methods is nearly the same both for the two different weighting factors. Even as T becomes larger, throughput gap between the two algorithms remains quite small. For $T = 80s$ under $\beta_1 = 1, \beta_2 = 1/10$, the run time for the SCA-based method is 3.7 minutes, but for the POA-based method is nearly 27 hours. This indicates that the SCA based method can achieve nearly the same optimal performance of the POA-based method while with much lower computational complexity.

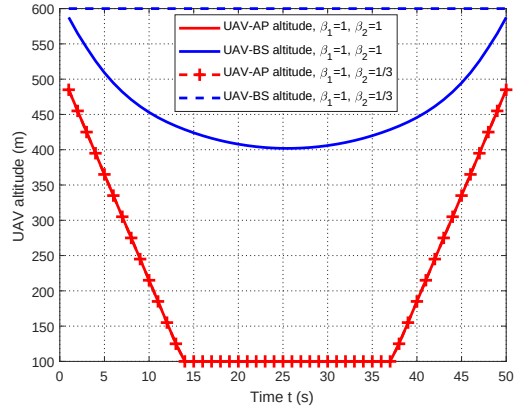

Fig. 4. Optimized UAV altitudes for different weighting factors when $T = 50s$.

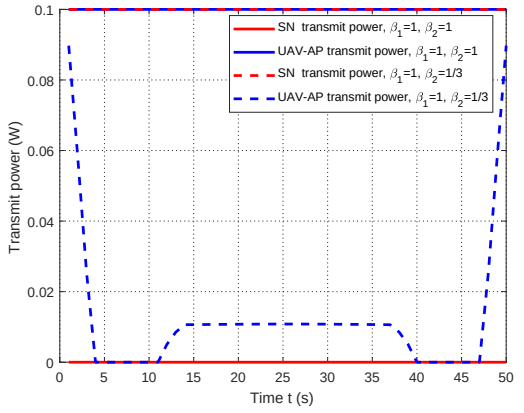

Fig. 5. Optimized SN/UAV-AP transmit power for different weighting factors when $T = 50s$.

B. Single SN and single AP case

We first consider a simple case where the UAV-BS collects data from one SN, and the UAV-AP transmits its data to one AP. Evidently, we do not need to consider communication scheduling in this case, and we only focus on designing the UAV trajectory and SN/UAV-AP transmit power.

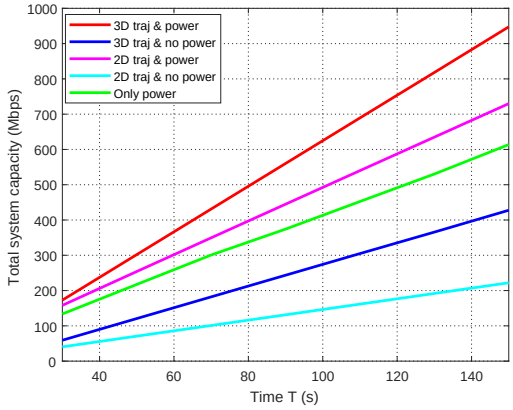

Fig. 6. System throughput versus period time T for weighing factors $\beta_1 = 1$ and $\beta_2 = 1/3$ for different benchmarks.

In Fig. 3, we plot the UAV-BS and UAV-AP 2D trajectories obtained by the SCA method for different weighting factors β_2=1 and β_2=1/3 when $T = 50s$. The initial locations of the UAV-AP and UAV-BS are $\mathbf{q}_{I_u}$=[0 300m] and $\mathbf{q}_{I_b}$=[0 700m], respectively. The final locations of the UAV-AP and UAV-BS are $\mathbf{q}_{F_u}$=[1000m 300m] and $\mathbf{q}_{F_b}$=[1000m 700m], respectively. The location of the SN and AP are set to [500m 550m] and [500m 450m], respectively. It is observed that both UAVs remain separated from each other to alleviate the interference received by the UAV-BS from the UAV-AP. In addition, as β_2 becomes smaller, the UAV-BS prefers moving closer to the SN, since the UAV-BS system throughput can be significantly improved by establishing a better channel between the UAV-BS and the SN. In addition, the UAV-AP tends to move far from the UAV-BS to reduce the interference imposed on the UAV-BS-based network.

To elaborate more clearly, the altitudes of the UAV-BS and UAV-AP are plotted in Fig. 4, with initial/final altitudes set as 600m and 500m, respectively. For $\beta_1 = 1$ and $\beta_2 = 1$, it can be seen that both UAVs descend to reduce the path loss and improve the system throughput.

In Fig. 5, the corresponding transmit power of the SN and UAV-AP is plotted. For $\beta_1 = 1$ and $\beta_2 = 1$, the UAV-AP transmits with maximum power while the SN remains 'mute', which implies that the UAV-BS system throughput is zero. However, with a smaller weight factor $\beta_2 = 1/3$, the SN transmits with maximum power while the UAV-AP transmit power is reduced, indicating that the UAV-BS system throughput can be improved by appropriately reducing β_2.

In Fig. 6, we investigate the total system throughput versus period T for different benchmarks to show the superiority of our proposed scheme. The definitions of the abbreviations of the benchmarks are given as below:

- **3D traj & power:** This is our proposed scheme that jointly optimizes the 3D UAV trajectory and communication design.
- **3D traj & no power:** The 3D UAV trajectory and communication scheduling are jointly optimized, but the transmit power is fixed at maximum power $p^s_{\max} = p^u_{\max} = 0.1$W.
- **2D traj & power:** The UAV altitude is fixed (here, the altitudes of the UAV-BS and UAV-AP are set to 600m and 500m, respectively), the horizontal UAV trajectory and communication design are jointly optimized.
- **2D traj & no power:** The 2D UAV trajectory and communication scheduling are jointly optimized, but the transmit power of the UAV/SN and altitude of the UAV are fixed ($p^s_{\max} = p^u_{\max} = 0.1$W, $H_b[n] = 600$m, $H_u[n] = 500$m).
- **Only power:** The UAV horizontal trajectory and altitude are predetermined ($H_b[n] = 600$m, $H_u[n] = 500$m), the horizontal trajectory for the UAV-AP/UAV-BS is a straight line from its initial location to its final location with constant speed). However, the communication design, including communication scheduling and transmit power, is optimized.

First, we observe that our proposed scheme is superior to the other benchmarks and achieves significant throughput gains, especially when the period becomes larger. Second, the system throughput can be improved by controlling the UAV altitude. For instance, for period $T = 130s$, the system throughput for the proposed scheme is 818Mbps, and for the "2D trajectory & power" method is 634Mbps, which provides nearly a 23% increase. In addition, the system throughput can be significantly improved by controlling the transmit power. For example, for period $T = 130s$, the system throughput for the "3D trajectory & no power" method is 365Mbps, and for the "2D trajectory & no power" method is 191Mbps, which correspond to a 55% and 76% increase in the system throughput, respectively. Finally, the UAV trajectory design also has significantly impacts on the system performance. For example, for period $T = 130s$, the system throughput for the "only power" method is 530Mbps, which results in a 35% decrease in the system throughput compared with our proposed method.

C. Multiple SNs and multiple APs case

In this section, we consider a more practical case where the UAV-BS and UAV-AP simultaneously serve multiple SNs and APs. The communication design, including power control and communication scheduling, and UAV trajectory are optimized. The impact of the weighting factors, UAV trajectory, transmit power are simulated to reveal some useful insights.

A. Optimized UAV trajectory and communication design using SCA method

In Fig. 7, we show the impact of UAV altitude and transmit power on the optimized UAV trajectories for different methods assuming four SNs and four APs. The SN and AP locations, and the initial UAV trajectories are same as in Section. A. Comparing Fig. 7 (a) with Fig. 7 (b), it can be seen that the obtained UAV trajectories for the UAV-BS and UAV-AP are almost the same. The corresponding transmit power is plotted in Fig. 10 (a), where we see that the optimized transmit power obtained by our proposed scheme either equals the maximum transmit value or zero, which means that nearly the same performance can be achieved for the "3D traj & no power" method by optimizing the communication scheduling.

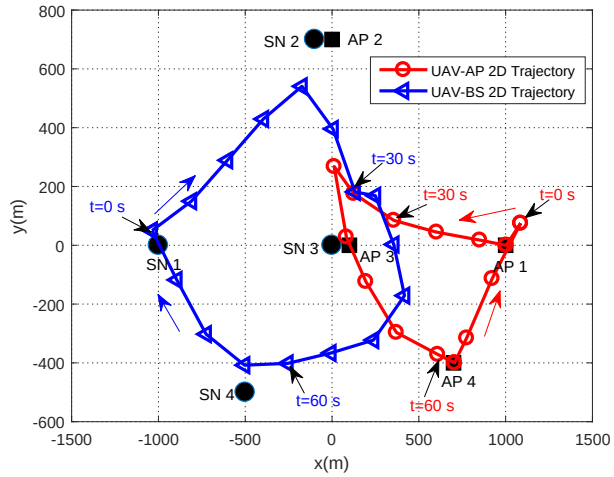

(a) Joint 3D UAV trajectory and power control optimization.

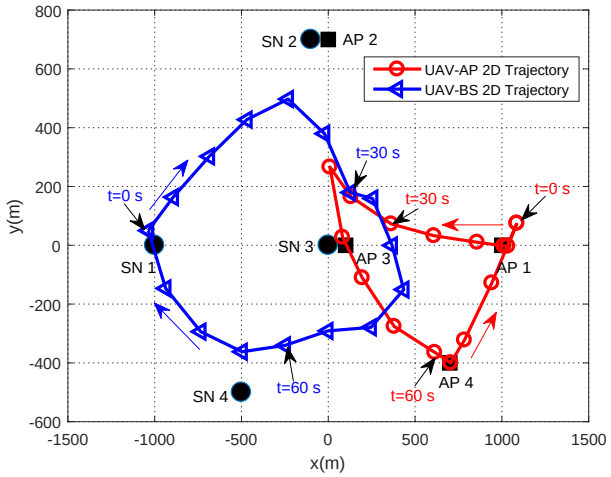

(b) 3D UAV trajectory without power control.

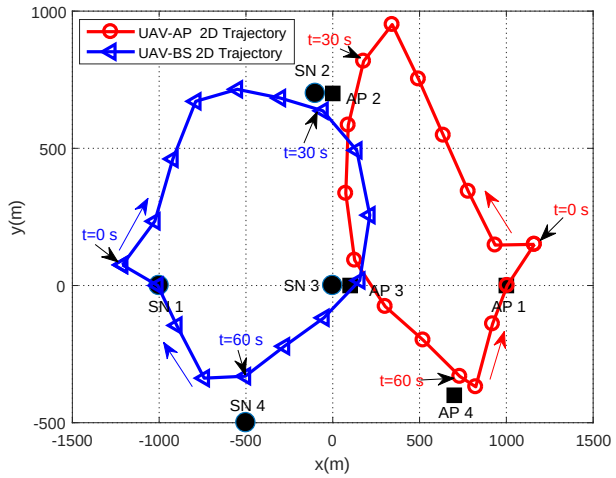

(c) Joint 2D UAV trajectory and power control optimization.

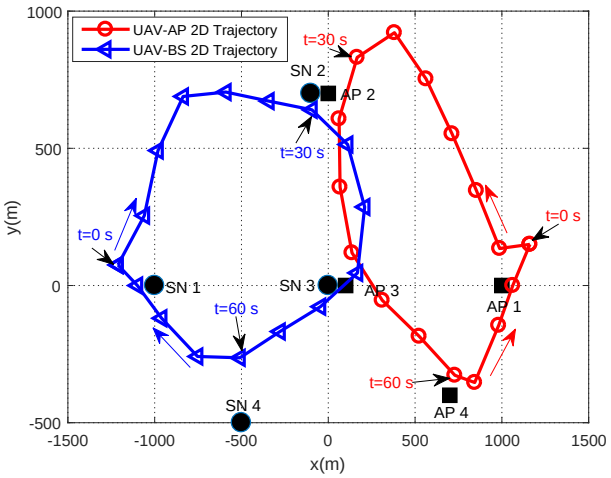

(d) 2D UAV trajectory without power control.

Fig. 7. UAV trajectories for different designs for the weighting factors $\beta_1 = \beta_2 = 1$ and $T = 80s$. Each trajectory is sampled every 5 seconds with the blue left arrow $\triangleleft$ marking the UAV-BS trajectory and the red circle $\circ$ marking the UAV-AP trajectory.

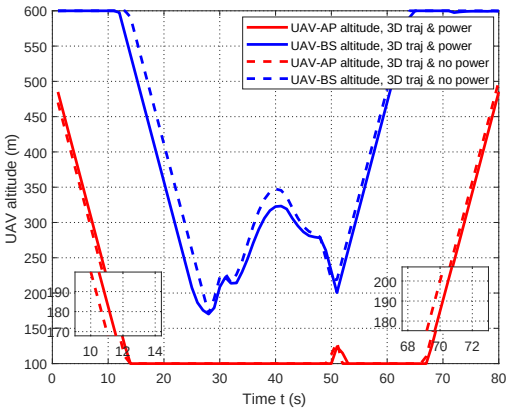

Fig. 8. UAV altitudes for different designs under the weight factors $\beta_1 = \beta_2 = 1$ and $T = 80s$.

In addition, the optimized UAV altitude is plotted in Fig. 8. It is observed that the obtained UAV altitudes are almost the same for both methods. This again demonstrates that the power control has little influence on the system performance for the weighting factors $\beta_1 = 1$ and $\beta_2 = 1$. We observe similar behavior comparing Fig. 7 (c) with Fig. 7 (d). However, the obtained trajectories for Fig. 7 (a) with Fig. 7 (c) (or Fig. 7 (b) with Fig. 7 (d)) are distinct, which means that the UAV altitude significantly influences the horizontal trajectory.

In Fig. 9, the UAV speed is plotted. It is observed that the UAV flies either with maximum horizontal speed or zero. In addition, unlike Fig. 9(c) or Fig. 9(d) where both of the UAV-AP and UAV-BS fly with maximum horizontal speed for nearly the whole period T in Fig. 9 (a) or Fig. 9(b), there is a large amount of time during which the two UAVs remain stationary. This is because exploiting the UAV altitude provides an additional degree of freedom for performance enhancement.

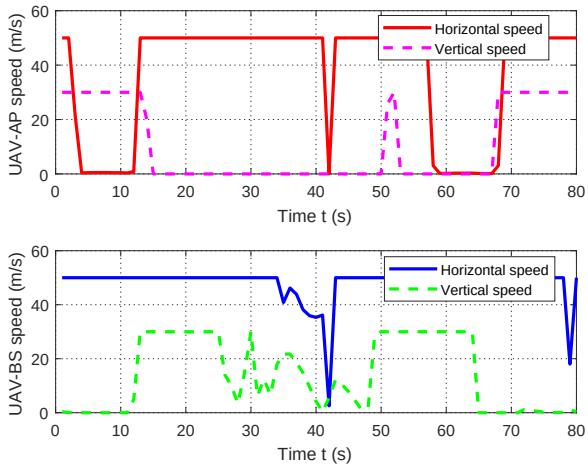

(a) Joint 3D UAV trajectory and power control optimization.

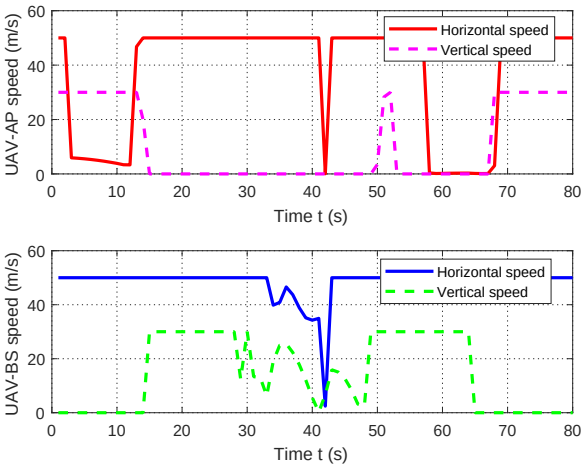

(b) 3D UAV trajectory without power control.

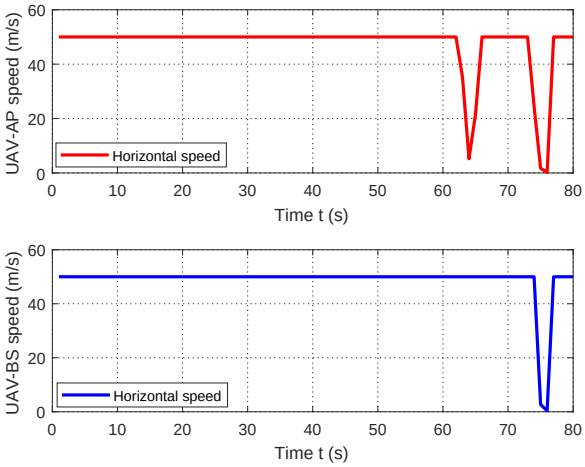

(c) Joint 2D UAV trajectory and power control optimization.

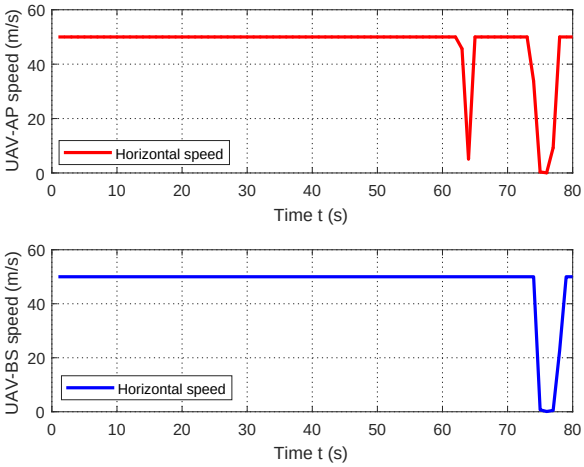

(d) 2D UAV trajectory without power control.

Fig. 9. UAV speed for different designs for the weighting factors $\beta_1 = \beta_2 = 1$ and $T = 80s$.

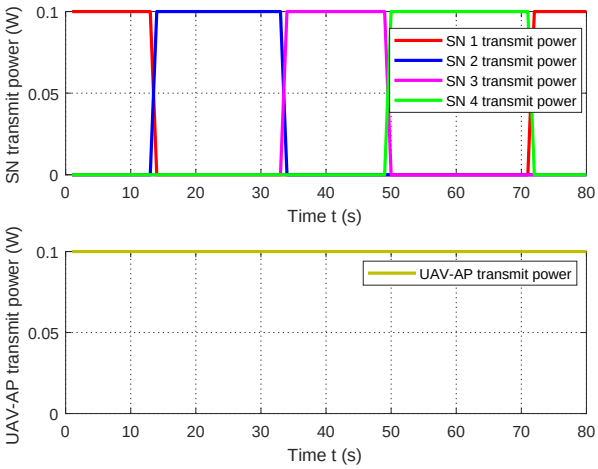

(a) Joint 3D UAV trajectory and power control optimization.

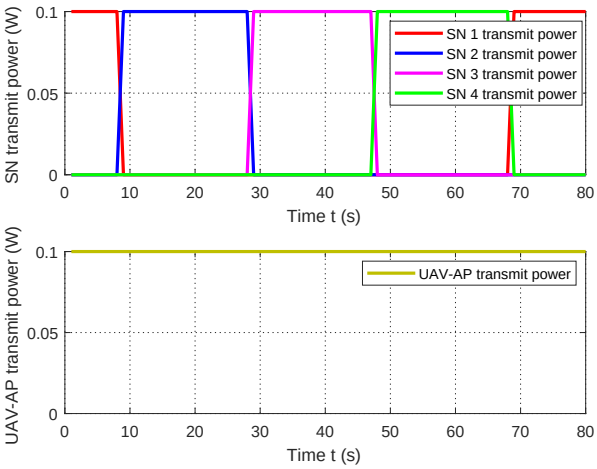

(b) Joint 2D UAV trajectory and power control optimization.

Fig. 10. Transmit power for different approaches with the weighting factors $\beta_1 = \beta_2 = 1$ and $T = 80s$.

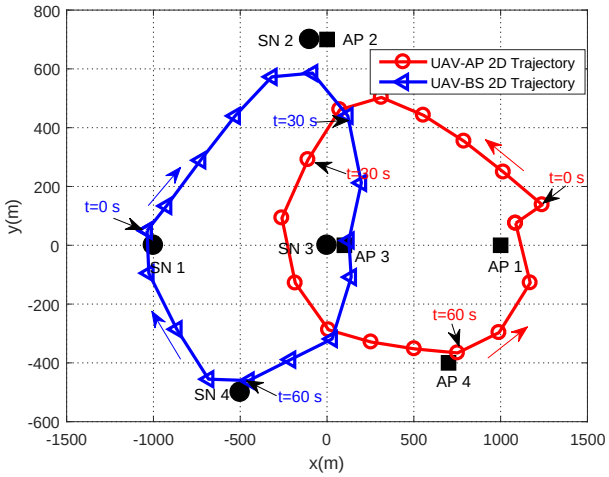

(a) Optimized UAV trajectories.

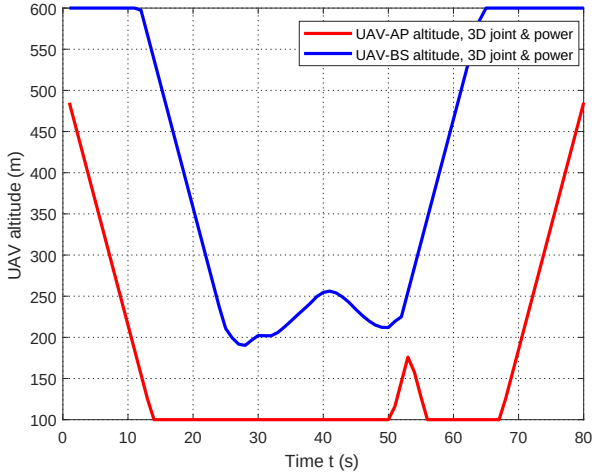

(b) Optimized UAV altitude

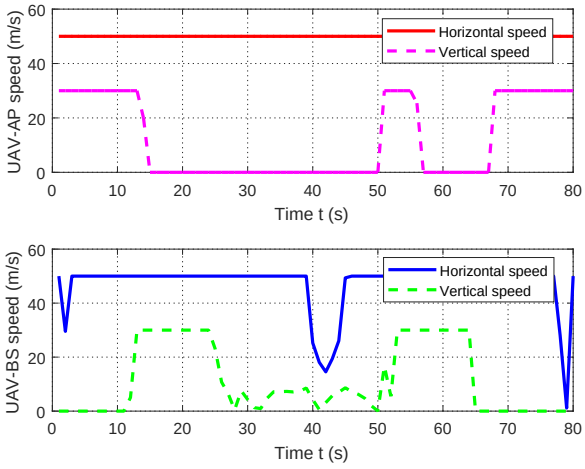

(c) Optimized UAV speed

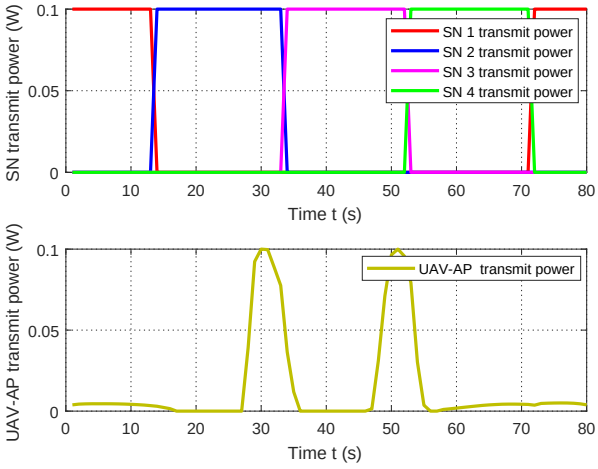

(d) Optimized UAV transmit power

Fig. 11. The UAV trajectory and communication designs obtained by using SCA method for $\beta_1 = 1$, $\beta_2 = 1/10$ when $T = 80s$.

Fig. 10 shows the transmit power for the "3D traj & power" and "2D traj & power" approaches. It can be seen that the UAV-AP always transmits with maximum power, and the SNs transmit either with maximum power or zero. This result indicates that the UAV-AP network has a higher priority than the UAV-BS network. Below we discuss the influence of the weighting factor β_2 on the system performance.

B. The impact of the weighting factors

The weighting factor β_2 is set to $\beta_2 = 1/10$ and β_1 as 1. The 3D UAV trajectory, speed, and transmit power are evaluated to show the impact of the weighting factors.

We see from Fig. 11 (a) with Fig. 7 (a) that the optimized UAV trajectory for the case of $\beta_1 = 1$ and $\beta_2 = 1/10$ is different from that for the case of $\beta_1 = 1$ and $\beta_2 = 1$. In Fig. 11 (a), both UAVs prefer to move closer to SN 2 or AP 2, respectively, and the trajectories are smoother than in Fig. 7 (a). In addition, unlike Fig. 10 (a) where the UAV-AP transmits with maximum power during the entire period. In Fig. 11 (d), the UAV-AP transmits with maximum power only from $t = 28s$ to $t = 35s$ and $t = 48s$ to $t = 55s$, and no power is transmitted during other times.

C. System performance

In Fig. 12, we compare our proposed design with different benchmarks for the different weighting factors in terms of system throughput. The UAV-AP, UAV-BS, and the total system throughput are respectively shown in Fig. 12 (a), Fig. 12 (b), and Fig. 12 (c), and they provide three useful insights. First, we see that our proposed scheme significantly outperforms the other benchmarks as shown in Fig. 12 (c). For example, for period $T = 120s$ and $\beta_2 = 1$, the total system throughput for the proposed scheme is 1551Mbps, which is 30% higher than for "3D traj & no power" (1074 Mbps), 20% higher than "2D traj & power" (1245 Mbps), 50% higher than "2D traj & no power" (777 Mbps), and 27% higher than the "only power" (1122 Mbps) algorithm. This means that the joint optimization of the 3D UAV trajectory and power control can indeed enhance the system performance. Second, the optimization of the power control provides a more pronounced

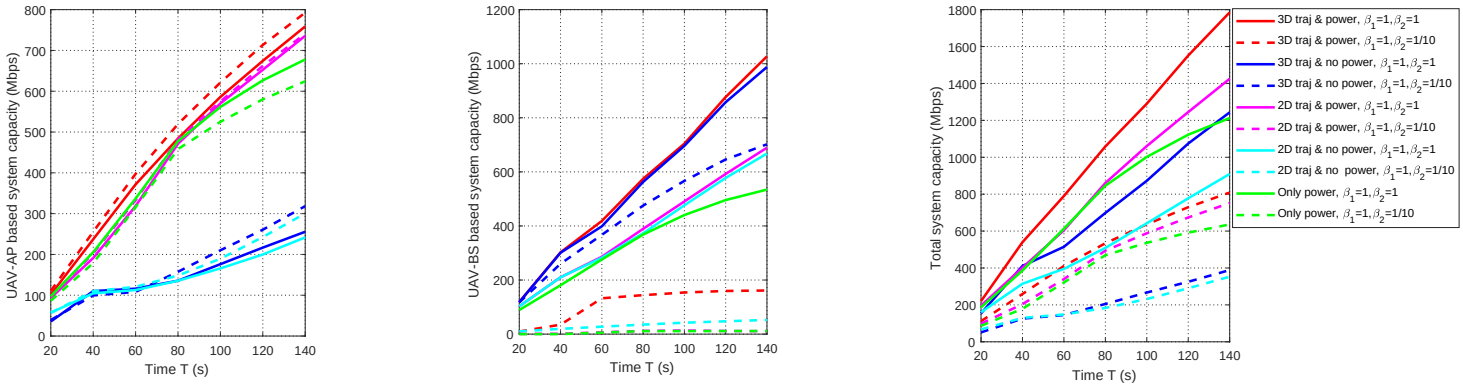

(a) UAV-AP based system throughput (b) UAV-BS based system throughput (c) Total system throughput

Fig. 12. System throughputversus period T for different benchmarks under different weighting factors.

improvement than the UAV trajectory optimization for our simulated scenario. Third, a larger weighting factor β_2 results in a higher system throughput.

VI. Conclusion

This paper studied the UAV-aided simultaneous uplink and downlink transmission networks, where one UAV-AP migrated data to the APs, and one UAV-BS collected data from the SNs. First, we considered a scenario where the two UAV trajectories were pre-determined, and the system throughput was maximized by leveraging the polyblock outer approximation method. Second, we developed a 3D trajectory and communication design approach for maximizing the system throughput, and a locally optimal solution was achieved by applying the successive convex approximation method. Numerical results showed that the proposed successive convex approximation method achieved nearly the same system throughput compared with the polyblock outer approximation method when the UAVs trajectory were pre-determined. In addition, compared with the benchmarks, a significant system throughput gain was obtained by optimizing the 3D UAV trajectory as well as the transmit power. This work can be extended by considering multiple UAV-BSs and UAV-APs. The additional interference caused by additional UAV-BS and UAV-AP should be carefully managed in order to maximize the system throughput.

Appendix A
Proof of Theorem 1

We prove Theorem 1 in two steps. In the first step, we show that the optimal SN transmit power (UAV-AP transmit power) for problem (11) results in at most one SN (AP) being active in each time slot. Define $\check{R}_k^s[n]$ as

$$\check{R}_k^s[n] = \log_2\left(1 + \frac{h_k\left[n\right]\tilde{p}_k^s\left[n\right]}{M\sum_{i\neq k}^{K}\tilde{p}_i^s\left[n\right] + \sum_{l=1}^{L} f\left[n\right]\tilde{p}_l^u\left[n\right] + \sigma^2}\right). \tag{45}$$

Suppose that more than one SN is active, and assume that there is K_1 number of SNs whose transmit power are non-zero, define $\tilde{p}_k^s[n] \neq 0$ for $k = 1, ..., K_1$ $(2 \leq K_1 \leq K)$ and $\tilde{p}_k^s[n] = 0$ for $k = K_1 + 1, ..., K$. Obviously, for $\forall k \in \{K_1 + 1, ..., K\}$, $\check{R}_k^s[n] = 0$. For $\forall k \in \{1, ..., K_1\}$ with a sufficiently large penalty factor $M \gg 1$, $M\sum_{i\neq k}^{K}\tilde{p}_i^s\left[n\right] \to \infty$. Thus, $\sum_{k=1}^{K}\check{R}_k^s\left[n\right] = 0$ at any time slot n.

Suppose that there is only one SN whose transmit power is non-zero. We assume that $\tilde{p}_1^s[n] \neq 0$ and $\tilde{p}_k^s[n] = 0$ for $k = 2, ..., K$. We have

$$\sum_{k=1}^{K} R_k^s\left[n\right] = \log_2\left(1 + \frac{h_1\left[n\right]\tilde{p}_1^s\left[n\right]}{\sum_{l=1}^{L} f\left[n\right]\tilde{p}_l^u\left[n\right] + \sigma^2}\right) > 0. \tag{46}$$

Therefore, we can declare that at most one SN is active in order to maximize (11).

Similarly, define

$$\check{R}_l^u[n] = \log_2\left(1 + \frac{g_l[n]\tilde{p}_l^u\left[n\right]}{M\sum_{i\neq l}^{L}\tilde{p}_i^u\left[n\right] + \sum_{k=1}^{K}\tilde{h}_{k,l}\tilde{p}_k^s\left[n\right] + \sigma^2}\right). \tag{47}$$

It is not difficult to verify that at most one AP can be active in order to maximize (11), based on the same derivation as in (45).

In the second step, we show that (11) is equivalent to (10). First, it can be easily seen that the optimal solution to problem (10) is feasible for problem (11) with the same objective value. Second, based on the first step, we see that the optimal solution to problem (11) is also feasible for problem (10) with same objective value.

This thus completes the proof of Theorem 1.

References

[1] A. prime air, "Overview of the Amazon prime air delivery drone concept," *https://www.amazon.com/Amazon-Prime-Air/b?ie=UTF8&node=8037720011*, 2019.

[2] Y. Zeng, R. Zhang, and T. J. Lim, "Wireless communications with unmanned aerial vehicles: Opportunities and challenges," *IEEE Communications Magazine*, vol. 54, no. 5, pp. 36–42, 2016.

[3] F. Jiang and A. L. Swindlehurst, "Optimization of UAV heading for the ground-to-air uplink," *IEEE Journal on Selected Areas in Communications*, vol. 30, no. 5, pp. 993–1005, 2012.

[4] Z. Han, A. L. Swindlehurst, and K. R. Liu, "Optimization of MANET connectivity via smart deployment/movement of unmanned air vehicles," *IEEE Transactions on Vehicular Technology*, vol. 58, no. 7, pp. 3533–3546, 2009.

[5] G. Zhang, Q. Wu, M. Cui, and R. Zhang, "Securing UAV communications via joint trajectory and power control," *IEEE Transactions on Wireless Communications*, vol. 18, no. 2, pp. 1376–1389, 2019.

[6] Q. Wu and R. Zhang, "Common throughput maximization in UAV-enabled ofdma systems with delay consideration," *IEEE Transactions on Communications*, vol. 66, no. 12, pp. 6614–6627, 2018.

[7] Q. Song, F.-C. Zheng, Y. Zeng, and J. Zhang, "Joint beamforming and power allocation for UAV-enabled full-duplex relay," *IEEE Transactions on Vehicular Technology*, vol. 68, no. 2, pp. 1657–1671, 2018.

[8] X. Li, H. Yao, J. Wang, X. Xu, C. Jiang, and L. Hanzo, "A near-optimal UAV-aided radio coverage strategy for dense urban areas," *IEEE Transactions on Vehicular Technology*, vol. 68, no. 9, pp. 9098–9109, 2019.

[9] X. Zhou, Q. Wu, S. Yan, F. Shu, and J. Li, "UAV-enabled secure communications: Joint trajectory and transmit power optimization," *IEEE Transactions on Vehicular Technology*, vol. 68, no. 4, pp. 4069–4073, 2019.

[10] Y. Zeng, Q. Wu, and R. Zhang, "Accessing from the sky: A tutorial on UAV communications for 5G and beyond," *Proceedings of the IEEE*, vol. 107, no. 12, pp. 2327–2375, 2019.

[11] I. Jawhar, N. Mohamed, J. Al-Jaroodi, and S. Zhang, "A framework for using unmanned aerial vehicles for data collection in linear wireless sensor networks," *Journal of Intelligent & Robotic Systems*, vol. 74, no. 1-2, pp. 437–453, 2014.

[12] M. Dong, K. Ota, M. Lin, Z. Tang, S. Du, and H. Zhu, "UAV-assisted data gathering in wireless sensor networks," *The Journal of Supercomputing*, vol. 70, no. 3, pp. 1142–1155, 2014.

[13] C. Zhan, Y. Zeng, and R. Zhang, "Energy-efficient data collection in UAV enabled wireless sensor network," *IEEE Wireless Communications Letters*, vol. 7, no. 3, pp. 328–331, 2018.

[14] Y. Zeng, J. Lyu, and R. Zhang, "Cellular-connected UAV: Potential, challenges, and promising technologies," *IEEE Wireless Communications*, vol. 26, no. 1, pp. 120–127, 2018.

[15] S. Zhang, Y. Zeng, and R. Zhang, "Cellular-enabled UAV communication: A connectivity-constrained trajectory optimization perspective," *IEEE Transactions on Communications*, vol. 67, no. 3, pp. 2580–2604, 2018.

[16] S. Zhang, H. Zhang, B. Di, and L. Song, "Cellular UAV-to-X communications: Design and optimization for multi-UAV networks," *IEEE Transactions on Wireless Communications*, vol. 18, no. 2, pp. 1346–1359, 2019.

[17] M. Alzenad, A. El-Keyi, and H. Yanikomeroglu, "3-D placement of an unmanned aerial vehicle base station for maximum coverage of users with different QoS requirements," *IEEE Wireless Communications Letters*, vol. 7, no. 1, pp. 38–41, 2017.

[18] A. Al-Hourani, S. Kandeepan, and S. Lardner, "Optimal LAP altitude for maximum coverage," *IEEE Wireless Communications Letters*, vol. 3, no. 6, pp. 569–572, 2014.

[19] M. Mozaffari, W. Saad, M. Bennis, and M. Debbah, "Efficient deployment of multiple unmanned aerial vehicles for optimal wireless coverage," *IEEE Communications Letters*, vol. 20, no. 8, pp. 1647–1650, 2016.

[20] J. Wang, C. Jiang, Z. Wei, C. Pan, H. Zhang, and Y. Ren, "Joint UAV hovering altitude and power control for space-air-ground IoT networks," *IEEE Internet of Things Journal*, vol. 6, no. 2, pp. 1741–1753, 2018.

[21] H. Dai, H. Zhang, M. Hua, C. Li, Y. Huang, and B. Wang, "How to deploy multiple uavs for providing communication service in an unknown region?" *IEEE Wireless Communications Letters*, vol. 8, no. 4, pp. 1276–1279, 2019.

[22] Y. Zeng and R. Zhang, "Energy-efficient UAV communication with trajectory optimization," *IEEE Transactions on Wireless Communications*, vol. 16, no. 6, pp. 3747–3760, 2017.

[23] C. You and R. Zhang, "3D trajectory optimization in Rician fading for UAV-enabled data harvesting," *IEEE Transactions on Wireless Communications*, vol. 18, no. 6, pp. 3192–3207, 2019.

[24] Y. Sun, D. Xu, D. W. K. Ng, L. Dai, and R. Schober, "Optimal 3D-trajectory design and resource allocation for solar-powered UAV communication systems," *IEEE Transactions on Communications*, vol. 67, no. 6, pp. 4281–4298, 2019.

[25] Q. Wu, Y. Zeng, and R. Zhang, "Joint trajectory and communication design for multi-UAV enabled wireless networks," *IEEE Transactions on Wireless Communications*, vol. 17, no. 3, pp. 2109–2121, 2018.

[26] M. Hua, Y. Wang, Q. Wu, H. Dai, Y. Huang, and L. Yang, "Energy-efficient cooperative secure transmission in multi-UAV enabled wireless networks," *IEEE Transactions on Vehicular Technology,doi: 10.1109/TVT.2019.2924180*, 2019.

[27] M. Hua, L. Yang, C. Pan, and A. Nallanathan, "Throughput maximization for full-duplex UAV aided small cell wireless systems," *IEEE Wireless Communications Letters, early access*, 2019.

[28] L. Qualcomm, "Unmanned aircraft systems-trial report-v1.0.1," 2017.

[29] 3GPP, "Enhanced LTE support for aerial vehicles," accessed on Jul. 16, 2017, [Online] Available: ftp://www.3gpp.org/specs/archive/36_series/36.777.

[30] J. Xu, Y. Zeng, and R. Zhang, "UAV-enabled wireless power transfer: Trajectory design and energy optimization," *IEEE Transactions on Wireless Communications*, vol. 17, no. 8, pp. 5092–5106, 2018.

[31] J. Lyu, Y. Zeng, and R. Zhang, "UAV-aided offloading for cellular hotspot," *IEEE Transactions on Wireless Communications*, vol. 17, no. 6, pp. 3988–4001, 2018.

[32] F. Zhou, Y. Wu, R. Q. Hu, and Y. Qian, "Computation rate maximization in UAV-enabled wireless-powered mobile-edge computing systems," *IEEE Journal on Selected Areas in Communications*, vol. 36, no. 9, pp. 1927–1941, 2018.

[33] M. Hua, Y. Wang, Z. Zhang, C. Li, Y. Huang, and L. Yang, "Power-efficient communication in UAV-aided wireless sensor networks," *IEEE Communications Letters*, vol. 22, no. 6, pp. 1264–1267, 2018.

[34] Q. Wu, J. Xu, and R. Zhang, "Capacity characterization of UAV-enabled two-user broadcast channel," *IEEE Journal on Selected Areas in Communications*, vol. 36, no. 9, pp. 1955–1971, 2018.

[35] J. Lyu, Y. Zeng, and R. Zhang, "Cyclical multiple access in UAV-aided communications: A throughput-delay tradeoff," *IEEE Wireless Communications Letters*, vol. 5, no. 6, pp. 600–603, 2016.

[36] H. Tuy, "Monotonic optimization: Problems and solution approaches," *SIAM Journal on Optimization*, vol. 11, no. 2, pp. 464–494, 2000.

[37] Y. J. A. Zhang, L. Qian, J. Huang *et al.*, "Monotonic optimization in communication and networking systems," *Foundations and Trends® in Networking*, vol. 7, no. 1, pp. 1–75, 2013.

[38] A. Zappone, E. Björnson, L. Sanguinetti, and E. Jorswieck, "Globally optimal energy-efficient power control and receiver design in wireless networks," *IEEE Transactions on Signal Processing*, vol. 65, no. 11, pp. 2844–2859, 2017.

[39] S. Boyd and L. Vandenberghe, *Convex optimization*. Cambridge university press, 2004.

[40] H. Wang, J. Wang, G. Ding, J. Chen, Y. Li, and Z. Han, "Spectrum sharing planning for full-duplex UAV relaying systems with underlaid D2D communications," *IEEE Journal on Selected Areas in Communications*, vol. 36, no. 9, pp. 1986–1999, 2018.